MedChemComm

Accepted Manuscript

ROYAL SOCIETY OF CHEMISTRY

www.rsc.org/medchemcomm

	Lord, Christopher J.; The Institute of Cancer Research, The Breakthrough Breast Cancer Research Centre and CRUK Gene Function Laboratory

Design and discovery of 3-aryl-5-substituted-isoquinolin-1-ones as potent tankyrase inhibitors

Richard J.R. Elliott[1‡], Ashley Jarvis[2‡], Mohan B. Rajasekaran[3‡], Malini Menon[1‡], Leandra Bowers[1‡], Ray Boffey[2], Melanie Bayford[2], Stuart Firth-Clark[2], Rebekah Key[2], Rehan Aqil[2], Stewart B. Kirton[§], Dan Niculescu-Duvaz[4], Laura Fish[4], Filipa Lopes[4], Robert McLeary[4], Ines Trindade[1], Elisenda Vendrell[1], Felix Munkonge[1], Rod Porter[5], Trevor Perrior[2], Caroline Springer[4], Antony W. Oliver[3], Laurence H. Pearl[3], Alan Ashworth[1*] and Christopher J. Lord[1*]

[1] The Breakthrough Breast Cancer Research Centre and CRUK Gene Function Laboratory, The Institute of Cancer Research, London, UK; [2] Domainex, 162 Cambridge Science Park, Milton Road, Cambridge, UK; [3] CRUK DNA Repair Enzymes Group, Genome Damage and Stability Centre, University of Sussex, UK; [4] CRUK Centre for Cancer Therapeutics, The Institute of Cancer Research, London, UK; [5]RodPorterConsultancy, Ashwell, Herts, UK; [§]Department of Pharmacy, University of Hertfordshire, Herts, UK. * (C.L. & A.A.) The Institute of Cancer Research, 237 Fulham Road, London , SW3 6JB, UK. E-mail: Chris.Lord@icr.ac.uk, Alan.Ashworth@icr.ac.uk.

Abstract:

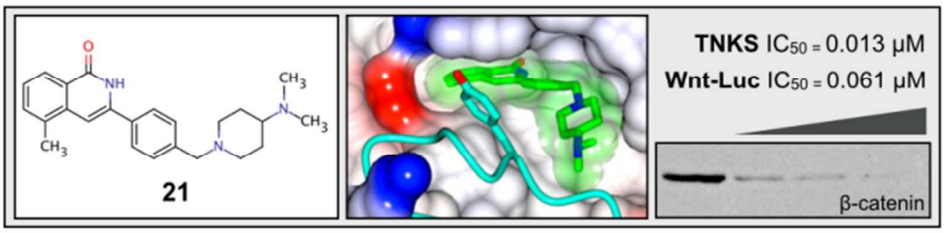

The tankyrase proteins (TNKS, TNKS2), members of the PARP superfamily of enzymes, are attractive anti-cancer drug targets, particularly as inhibition of their catalytic activity has been shown to antagonise oncogenic WNT signalling. To identify chemical inhibitors of tankyrase we carried out an *in silico* small molecule screen using a set of 'PARP-binding' pharmacophores together with a generated (liganded) tankyrase homology model. This approach identified a structurally diverse set of ~1000 compounds for further study. Subsequent in vitro screening of recombinant tankyrase protein identified a subset of 59 confirmed inhibitors. Early optimisation followed by cell-based studies in WNT-dependent tumour cells, as well as co-crystallisation studies, identified a novel class of 3-aryl-5-substituted isoquinolin-1-ones, such as **21**, that exhibit potent inhibition of tankyrase activity as well as growth inhibition of colorectal cancer cells.

Introduction

The ADP-ribosyltranferase diphtheria toxin-like (ARTD) or poly-ADP-ribose polymerase (PARP) protein superfamily comprises 17 proteins that contain a common catalytic domain. Those that are catalytically active use β-NAD^+ as an essential co-factor to transfer poly- or mono-ADP-ribose units onto protein substrates[1]. This post-translational modification is best characterised for PARP1 (ARTD1) and PARP2 (ARTD2) substrates, which play an important role in the DNA damage response. The PARP1/2 inhibitor olaparib has now been approved for use in the treatment of ovarian cancer, as it is able to selectively target tumour cells with either a BRCA1 or BRCA2 tumour suppressor gene defect[2]. PARP1/2 inhibitors such as olaparib **1** and veliparib **2** exploit the nicotinamidyl pharmacophore present in β-NAD^+ **3** (Supplementary **Figure 1**). Tankyrase 1 and 2 (TNKS/ARTD5 & TNKS2/ARTD6) are PARP proteins which are involved in a range of cellular functions including telomere maintenance, control of the mitotic checkpoint and WNT signalling, as well as the genetic disorder Cherubism[3].

The role of TNKS/TNKS2 in WNT signalling has highlighted the potential of tankyrase inhibitors as anti-cancer agents, as this pathway has been associated with the development of many tumour types, including colorectal cancers, where loss-of-function mutations in the tumour suppressor gene *APC*[4] cause constitutive WNT signalling driving a tumourigenic phenotype. APC acts as a molecular scaffold, or hub, for the assembly of the 'destruction complex', a key component of canonical WNT signalling; this complex, which includes GSK3β and AXIN1/2, sequesters cytosolic β-catenin (a known transcriptional co-activator). The subsequent phosphorylation of β-catenin, by GSK3β, promotes its degradation by the proteasome, leading to the inactivation of WNT signalling[3].

Conversely, loss of normal destruction complex function, which can occur when *APC* is mutated, leads to an enhanced level of nuclear, non-phosphorylated, 'active' β-catenin which then drives the transcription of WNT target genes such as *MYC*[5]. TNKS and TNKS2 normally PARylate two components of the destruction complex, AXIN1 and AXIN2, thereby promoting their ubiquitylation and proteosomal degradation; events that minimise the total amount of active β-catenin[6]. Inhibition of TNKS/TNKS2 minimises AXIN degradation, stabilises the destruction complex and suppresses WNT signalling[6]. As constitutive WNT signalling can often be oncogenic, chemical inhibitors of tankyrase activity have been proposed as potential anti-cancer agents[6].

Here we describe the design and discovery of a series of novel 3-aryl-5-substituted isoquinolin-1-one compounds that are potent TNKS/TNKS2 inhibitors. The optimised compounds presented in this study were characterised by their biochemical potency (estimated using an *in vitro* poly-ADP-ribosylation assay), their ability to inhibit cellular WNT signalling (quantified using a transcriptional reporter assay) and their ability to inhibit growth of WNT-dependent, *APC*-mutant (APC^{mut}) colorectal tumour cells.

Results and discussion

***In silico* and biochemical screening for TNKS inhibitors**. In order to initiate the discovery of small molecule TNKS/TNKS2 inhibitors, we used an *in silico* small molecule screen (**Supplementary Figure 2**) to identify a set of commercially available compounds that contained the core (nicotinamide-like) aryl-CONH unit found in PARP superfamily inhibitors such as olaparib **1** (AstraZeneca/KuDOS) and veliparib **2** (AbbVie) (**Supplementary Figure 1**). One thousand and sixty nine compounds were identified using this approach, which were then assessed using a cell free biochemical assay, where the ability to inhibit PARylation of a histone pseudo-substrate by recombinant TNKS was quantified[7, 8]. This analysis produced 59 hits with >75% inhibition of TNKS activity at a concentration of 10 μM (**Supplementary Figure 3**). Consequently, several robust chemical series were identified after dose response validation assays (data not shown) of which one, based on a dihydroisoquinolin-1-one (DHIQ) scaffold, was selected for further optimisation and derivatisation (for an example from the DHIQ series, Compound **4**, see **Supplementary Figure 1**).

Optimisation of hits from primary screening. At the very start of our studies, there were no confirmed tankyrase inhibitors, or publically available X-ray crystal structures of ligand-bound protein, so our initial optimisation of the DHIQ series depended on insights gleaned from *in silico* molecular docking studies (using a TNKS homology model that we had generated for our initial virtual screen; see **Supplementary Information** for description) together with structure-activity relationships (SAR) from our other hit series (data not shown). Shortly after the instigation of our studies, a structurally-related compound, XAV939 **5** (**Supplementary Figure 1**), was shown to antagonise WNT signalling by stabilising AXIN1/2 protein levels and was confirmed as a TNKS inhibitor[6], therefore we could also benefit from information contained in this chemical structure. In our design we sought to preserve the classical PARP1 binding motif in the nicotinamide-binding region [i.e. the H-bonding network between the lactam carbonyl O with Ser1221 (OH) and Gly1185 (NH) and also the lactam NH with Gly1185 (C=O)]. We also wanted to make use of the rich potential for pi-stacking and non-polar (hydrophobic) interactions found in the binding site in order to maximise the affinity of our compounds. Analysing how the DHIQ scaffold docked into the TNKS homology model allowed us to consider 'morphing' from DHIQ into a flattened isoquinolin-1-one (IQ) scaffold thereby optimising the pi-stacking interaction with Tyr1224. We further envisioned aryl substitution of the lactam-containing ring (XAV939 **5** contains an aryl-substituted lactam), with scope for growth *via* the *para*- position. We were aware that the isoquinolin-1-one scaffold had featured in PARP superfamily inhibitors, with examples that incorporated 5-substitution (Compound **4** possesses a 5-substituted $–OCH_2CONH$-aryl motif; **Supplementary Figure 1)**, but our planned 3-aryl substitution, and subsequent para-growth, afforded a unique, differentiating opportunity. Finally, we sought to replace the 'inefficient' $–OCH_2CONH$-aryl motif incorporated in **4** (**Supplementary Figure 1**) with a smaller group envisaged to be more compatible with the target protein. Our model for the proposed binding of an optimised IQ example, as represented by compound **11**, is shown in **Figure 1A**.

Structure-based drug design. Again, using docking to guide our design efforts, we prepared and tested a set of 3-aryl-isoquinolin-1-one compounds, which upon further optimisation, led to a preferred series of 3-aryl-5-substituted-isoquinolin-1-ones (**Table 1**) that showed

improved TNKS potency, especially when compared to **4**. Recently, a range of structurally diverse TNKS inhibitors have been reported[9,10,11,12]. In 2012, an X-ray crystal structure of XAV939 **5** bound to the nicotinamide-binding pocket of the catalytic domain of TNKS[13] reinforced the key features of the IQ binding model that we had envisaged (**Figure 1B**). Thus, with a now established and robust structure-based paradigm we turned our attention to progression of our hit compounds, designing a test cascade — beginning with the generation of dose response curves using recombinant TNKS in PARylation assays, then moving onto a cell-based WNT (LEF/TCF) luciferase reporter system that assessed ability to inhibit β-catenin driven mRNA transcription — to select promising compounds that were then assessed for their selectivity against PARP1.

Biological assessment of optimised compounds. The bioactivity SAR (**Table 1**) highlighted an important role for the R^1 group, with examples containing R^1 = OMe (compounds **10, 11, 12**) showing enhanced inhibition of the WNT-luciferase (WNT-Luc) signal, compared with R^1 = H, F and Cl (compounds **13, 14, 15** and **16**). Compound **11**, for example, not only showed good TNKS inhibitory activity but also demonstrated excellent selectivity over full length PARP1 (IC_{50} 7900 nM, >200-fold) and in DLD1 human colorectal tumour cells, inhibited WNT-reporter gene transcription with an IC_{50} = 59 nM. Unfortunately, other compound properties (where determined), such as aqueous solubility and microsomal stability, required improvement, although we found that the solubility could be greatly enhanced with the incorporation of an amine at R^2 (e.g. > 100 μM in phosphate-buffered saline at pH 7.4 for compounds **12** and **16** with R^2 = $-CH_2NMe_2$).

As one of our future aspirations was to be able to explore the pharmacological potential for tankyrase inhibitors using murine models of human cancer, we recognised that we would need to identify compounds that possessed an acceptable balance between potency and pharmacokinetic (PK) properties. Encouraged by our initial results, we prepared and tested a focused group of IQ compounds (**Table 2**) that combined R^1 = Me, included as a surrogate for the potent, but metabolically-labile, OMe group (O-demethylation was confirmed by metabolite identification using LC-MS), with R^2 = CH_2'N' (e.g. CH_2NMe_2). These compounds retained or enhanced the desired mechanistic (WNT pathway) cellular potency and were able to inhibit growth of an *APC*-mutant colorectal cell line, DLD1 (Table 2). In support of this observation, a recent report has indicated that a methyl group occupying a comparable (8-) position on a series of 2-arylquinazoline-4-one TNKS/TNKS2 inhibitor also enhances potency[14]. Furthermore, additional improvements were apparent, e.g. compound **21** had good aqueous solubility (> 100 μM in phosphate-buffered saline at pH 7.4) and demonstrated good metabolic stability upon exposure to mouse and human liver microsomes (MLM/HLM Cl_{int} = 10/5 μL/min/mg protein). Subsequent to this, using X-ray crystallographic studies, we sought to reinforce our understanding of the structural underpinnings for compound potency, and were able to determine the structure of compound **12** bound to TNKS at 3.4 Ångström resolution (see **Supplementary Information** for additional details). The binding mode of **12**, determined by crystallography, was comparable to that observed for XAV939 **5** and also to the optimum molecular docking pose determined with our TNKS homology model and compound **11** (**Figure 1A, B, C**). Furthermore, we then went on to determine crystal structures of **21** and **23** in complex with TNKS, at 2.4 and 2.5 Ångström respectively (**Figure 1D, E**).

Each of the three compounds made the same core set of hydrogen-bonds, i.e. from the NH and carbonyl groups of the isoquinolin-1-one scaffold, to the backbone carbonyl and NH of Gly1185, respectively. An additional interaction was also made to the hydroxyl group of the Ser1221 side chain. Furthermore, Tyr1203 of the 'D-loop' motif (amino acids Phe1197-Gly1211 – subsequently targeted as one of the primary areas to influence selectivity *vs*. PARP1,2[15]) as well as Tyr1213 and Tyr1224, were involved in van der Waals interaction with the bound compound; in particular Tyr1224 was pi-stacked up against the face of the isoquinolin-1-one core, as predicted from our original molecular modeling study (**Figure 1A**). When the **12, 21** and **23** co-crystal structures were overlaid, small movements in the position of the Phe1188 side chain were also evident (**Figure 1F**); this was concomitant with a van der Waals interactions of this side chain with the additional pendant rings of **21** and **23**, when compared to **12**, and may therefore provide a favorable interaction which contributes to the increased potency of these compounds. It is worth noting here that our TNKS homology model was built with the structural data available at the time, and so our docking poses did not fully account for the conformational flexibility of the D-loop region, and therefore did not predict the interaction of bound ligands with the side chain of, e.g. Tyr1203. This, however, did not seem to affect the validity of the docking poses generated.

Compounds were also assessed for their ability to stabilise both tankyrase and AXIN1/2 protein levels (by inhibiting auto-PARylation and substrate PARylation, respectively) and destabilise β-catenin (for example, **Figure 2A**, compound **21**). Upon testing **21** in a larger panel of tumour cell lines (**Figure 2B**), preferential potency against *APC*-mutant lines compared to non-*APC*-mutant lines was observed, suggesting that **21** would appear to be representative of a potent class of TNKS inhibitor, with favorable tumour cell inhibitory properties.

Whilst these cell inhibitory properties of **21** might only be partially due to TNKS inhibition, and possibly due to PARP1 or other PARP superfamily inhibitory effects (for example, the selectivity of **21** for TNKS over PARP1 in a cell free biochemical assay was only 35-fold), we noted that Compound **21** only impaired cellular DNA-damage induced (PARP1-mediated) PARylation at concentrations > 100 nM (**Supplementary Figure 4**). Furthermore, the PARP inhibitor olaparib **1** showed particularly poor activity in our WNT-luciferase assay (IC_{50} 3534 nM) and did not alter protein levels of AXIN1/2 or β-catenin and only affected TNKS stability at high concentrations (**Supplementary Figure 5A**, **B**). Cell lines expressing mutant APC were unaffected by olaparib **1** at concentrations that normally inhibit *BRCA1* or *BRCA2* mutant tumour cells (DLD1 SF_{50} 2000 nM, HT55 SF_{50} 6265 nM). So, whilst selectivity of a TNKS inhibitor against PARP1 may be desirable *per se*, any PARP1 inhibitory (off-target) effect is unlikely to have an impact on cell viability in *APC*-mutant colorectal cancer. However, since compound **21** was not assayed against the remaining PARP family members we cannot preclude the effect that complete or partial inhibition of these related enzymes may have on the viability of the cell line models tested.

Experimental

The synthesis of 3-aryl-5-methyl isoquinolin-1-one compounds **10-23** (see **Supplementary Information** for full experimental details) was achieved by the one-pot, lithiated toluamide-aryl nitrile cycloaddition method[16, 17] using toluamides **7a–7e** and 4-(R^2)-aryl nitriles (see **Scheme 1** for representative examples **11, 12, 17, 19, 21, 23**). The toluamides were either commercially available **7e** or prepared using a coupling reaction between substituted benzoic acids **6a-6d** and diethylamine. The 4-(R^2)-aryl nitriles **9a-9b** were prepared in moderate yield using a halide displacement reaction between 4-bromomethyl-benzonitrile **8** and the corresponding, commercially available secondary amines. The remaining 4-(R^2)-aryl nitriles (where R^2 = F, Me, CH_2NMe_2, CF_3, CH_2-N-morpholine, CH_2-N-(4-Me)-piperazine, CH_2-N-(4-Boc)-piperazine) were all commercially available.

Conclusions

In summary, we have described the discovery, optimisation and biological properties of a novel series of 3-aryl-5-substituted-isoquinolin-1-ones as potent inhibitors of the PARP superfamily enzyme, TNKS. In particular, a class of 3-aryl-5-methyl-isoquinolin-1-one compounds demonstrated enhanced potency in biochemical and cell-based assays as well as improved solubility and metabolic stability.

Notes and references:

For complete experimental details for the TNKS homology model generation and virtual screen, chemical synthesis, biological assays and X-ray crystallography see **Supplementary Information**. The PDB accession codes for the X-ray co-crystal structure of TNKS + **12**, TNKS + **21** and TNKS + **23** are 4UW1, 4U6A and 4UUH, respectively.

Acknowledgements

This work was funded by the Wellcome Trust as part of its Seeding Drug Discovery Initiative (SDDI, WT101816). The funders took no part in the drafting of this manuscript. The licensing or sale of intellectual property described in this paper may result in income that will be shared by the ICR and those who contributed directly to the intellectual property under the Institutes 'Rewards to Discovers Scheme'. Part of this work has been described in a PCT application published as WO2013/132253 A1**.**

1 M. Rouleau, A. Patel, M. J. Hendzel, S. H. Kaufmann and G. G. Poirier, *Nat Rev Cancer*, 2010, **10**, 293-301.
2 C. J. Lord and A. Ashworth, *Nature*, 2012, **481**, 287-294.
3 J. L. Riffell, C. J. Lord and A. Ashworth, *Nature reviews. Drug discovery*, 2012, **11**, 923-936.
4 S. M. Powell, N. Zilz, Y. Beazer-Barclay, T. M. Bryan, S. R. Hamilton, S. N. Thibodeau, B. Vogelstein and K. W. Kinzler, *Nature*, 1992, **359**, 235-237.
5 T. C. He, A. B. Sparks, C. Rago, H. Hermeking, L. Zawel, L. T. da Costa, P. J. Morin, B. Vogelstein and K. W. Kinzler, *Science*, 1998, **281**, 1509-1512.
6 S. M. Huang, Y. M. Mishina, S. Liu, A. Cheung, F. Stegmeier, G. A. Michaud, O. Charlat, E. Wiellette, Y. Zhang, S. Wiessner, M. Hild, X. Shi, C. J. Wilson, C. Mickanin, V. Myer, A. Fazal, R. Tomlinson, F. Serluca, W. Shao, H. Cheng, M. Shultz, C. Rau, M. Schirle, J. Schlegl, S. Ghidelli, S. Fawell, C. Lu, D. Curtis, M. W. Kirschner, C. Lengauer, P. M. Finan, J. A. Tallarico, T. Bouwmeester, J. A. Porter, A. Bauer and F. Cong, *Nature*, 2009, **461**, 614-620.
7 C. C. Clark, J. N. Weitzel and T. R. O'Connor, *Mol Cancer Ther*, 2012, **11**, 1948-1958.
8 M. Fraser, H. Zhao, K. R. Luoto, C. Lundin, C. Coackley, N. Chan, A. M. Joshua, T. A. Bismar, A. Evans, T. Helleday and R. G. Bristow, *Clin Cancer Res*, 2012, **18**, 1015-1027.
9 A. Voronkov, D. D. Holsworth, J. Waaler, S. R. Wilson, B. Ekblad, H. Perdreau-Dahl, H. Dinh, G. Drewes, C. Hopf, J. P. Morth and S. Krauss, *Journal of medicinal chemistry*, 2013, **56**, 3012-3023.
10 H. Bregman, N. Chakka, A. Guzman-Perez, H. Gunaydin, Y. Gu, X. Huang, V. Berry, J. Liu, Y. Teffera, L. Huang, B. Egge, E. L. Mullady, S. Schneider, P. S. Andrews, A. Mishra, J. Newcomb, R. Serafino, C. A. Strathdee, S. M. Turci, C. Wilson and E. F. DiMauro, *Journal of medicinal chemistry*, 2013, **56**, 4320-4342.
11 M. D. Shultz, A. K. Cheung, C. A. Kirby, B. Firestone, J. Fan, C. H. Chen, Z. Chen, D. N. Chin, L. Dipietro, A. Fazal, Y. Feng, P. D. Fortin, T. Gould, B. Lagu, H. Lei, F. Lenoir, D. Majumdar, E. Ochala, M. G. Palermo, L. Pham, M. Pu, T. Smith, T. Stams, R. C. Tomlinson, B. B. Toure, M. Visser, R. M. Wang, N. J. Waters and W. Shao, *Journal of medicinal chemistry*, 2013, **56**, 6495-6511.
12 P. Liscio, A. Carotti, S. Asciutti, T. Karlberg, D. Bellocchi, L. Llacuna, A. Macchiarulo, S. A. Aaronson, H. Schuler, R. Pellicciari and E. Camaioni, *Journal of medicinal chemistry*, 2014, **57**, 2807-2812.
13 C. A. Kirby, A. Cheung, A. Fazal, M. D. Shultz and T. Stams, *Acta crystallographica. Section F, Structural biology and crystallization communications*, 2012, **68**, 115-118.
14 A. Nathubhai, P. J. Wood, M. D. Lloyd, A. S. Thompson and M. D. Threadgill, *Acs Med Chem Lett*, 2013, **4**, 1173-1177.
15 E. Wahlberg, T. Karlberg, E. Kouznetsova, N. Markova, A. Macchiarulo, A-G. Thorsell, E. Pol, A. Frostell, T. Ekblad, D. Öncü, B. Kull, G. M. Robertson, R. Pellicciari, H. Schüler and J. Weigelt, *Nature Biotechnology*, 2012, **30**, 283-288.
16 W. J. Cho, S. J. Yoo, M. J. Park, B. H. Chung and C. O. Lee, *Archives of pharmacal research*, 1997, **20**, 264-268.
17 G. S. Poindexter, *J Org Chem*, 1982, **47**, 3787-3788.

Figure 1

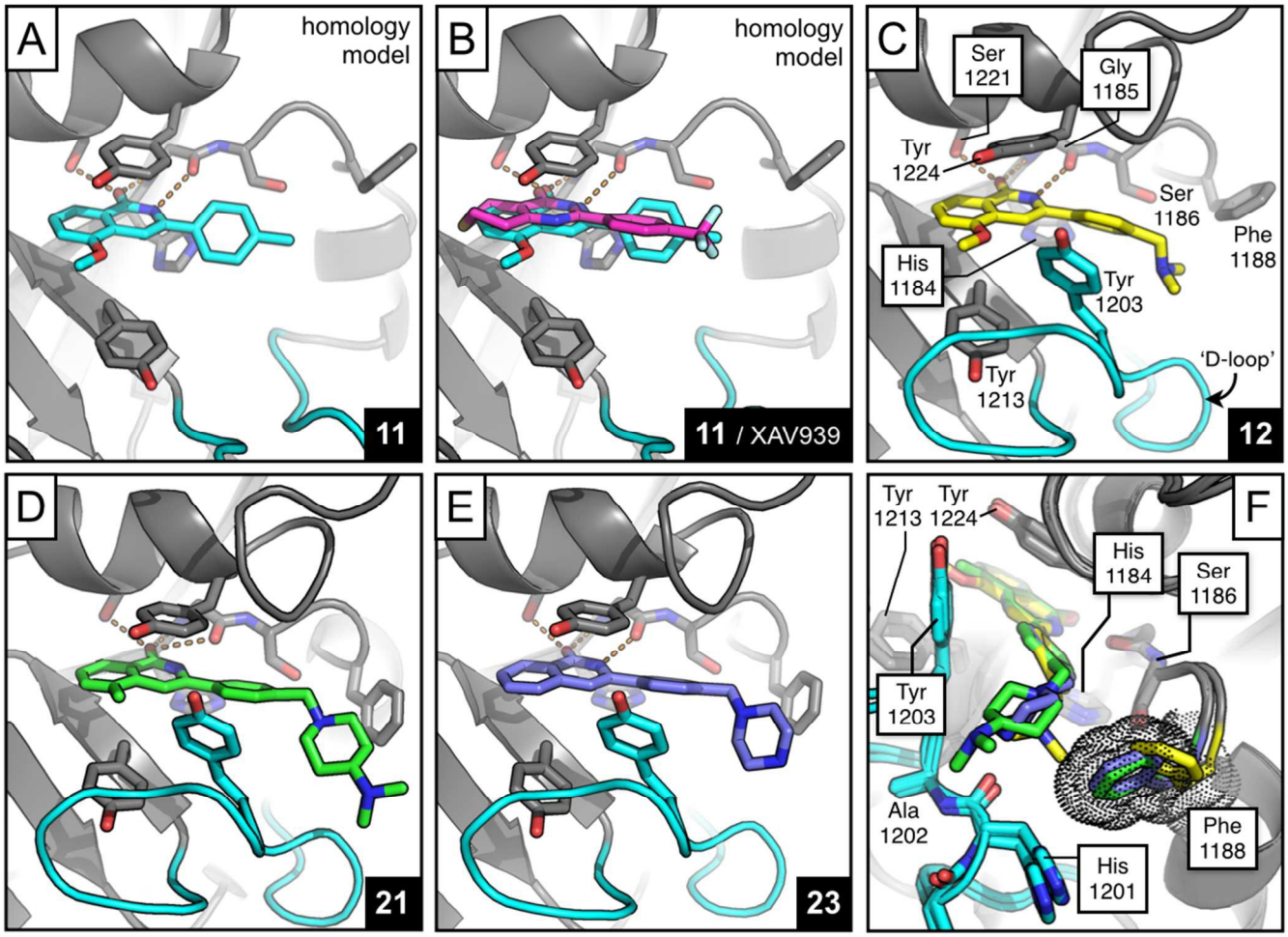

Figure 2

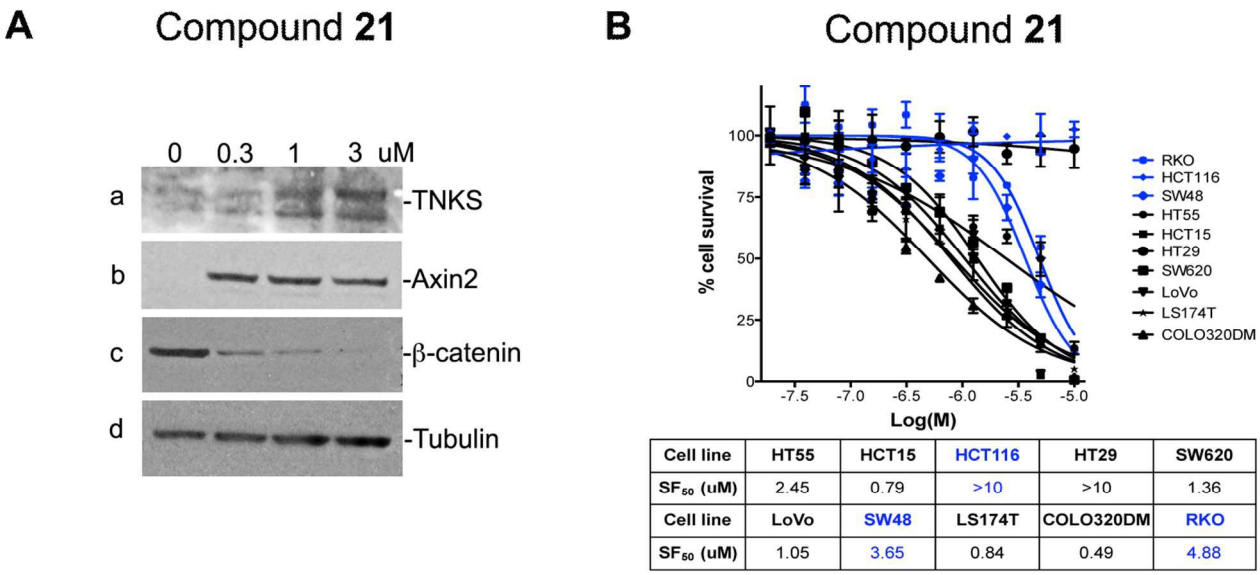

Cell line	HT55	HCT15	HCT116	HT29	SW620
SF_{50} (uM)	2.45	0.79	>10	>10	1.36
Cell line	LoVo	SW48	LS174T	COLO320DM	RKO
SF_{50} (uM)	1.05	3.65	0.84	0.49	4.88

Scheme 1.

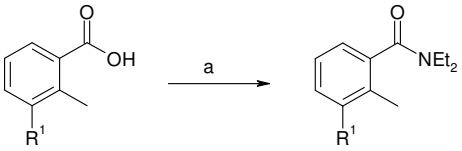

6a: R^1 = OMe
6b: R^1 = Cl
6c: R^1 = F
6d: R^1 = Me

7a: R^1 = OMe
7b: R^1 = Cl
7c: R^1 = F
7d: R^1 = Me

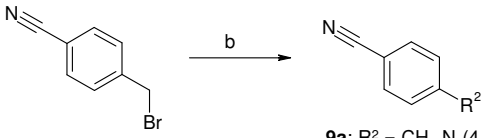

8

9a: R^2 = CH_2-N-(4-NMe_2)-piperidine
9b: R^2 = CH_2-N-(3-NMe_2)-azetidine

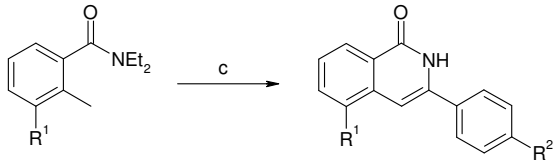

Compounds **10** - **23**, e.g.:

7a: R^1 = OMe
7b: R^1 = Cl
7c: R^1 = F
7d: R^1 = Me
7e: R^1 = H

11: R^1 = OMe, R^2 = Me
12: R^1 = OMe, R^2 = CH_2NMe_2
17: R^1 = Me, R^2 = CH_2NMe_2
19: R^1 = Me, R^2 = CH_2-N-(4-Boc)-piperazine
23: R^1 = Me, R^2 = CH_2-N-piperazine
21: R^1 = Me, R^2 = CH_2-N-(4-NMe_2)-piperidine

Figure Legends

Figure 1. (A) Representative docking pose for IQ compound **11** bound to the homology model of TNKS. (B) Predicted binding mode of **11** compared to that observed for XAV939 **5**. (C) Confirmation of the binding mode as determined by an X-ray co-crystal structure of **12** in complex with TNKS. (D) TNKS in complex with **21**. (E) TNKS in complex with **23**. (F) Overlay of each crystal structure, highlighting the movement of Phe1188 in each case (van der Waals radii represented by dotted surface). Potential hydrogen bonds to key amino acids (as labeled) are shown as orange dashed lines.

Figure 2. (A) Western blot illustrating effect on TNKS, AXIN2, β-catenin and Tubulin protein levels in SW480 colorectal tumour cells exposed to **21**. (B) Cell survival plots illustrating data from multiple colorectal tumour cell lines exposed to **21**. Cell lines with mutant *APC* alleles are indicated in black, and those with wild-type *APC* in blue. Error bars represent SEM from ≥3 replica experiments.

Scheme 1. Synthesis of Compounds **10-23**. Reagents and conditions: (a) Et_2NH, TBTU, DIPEA, DCM/DMF (1:1), rt or $(COCl)_2$, DCM, cat. DMF then Et_2NH, DCM, 0 ^oC to rt ; (b) 4-(Dimethylamino)piperidine, Et_3N, THF, 50 ^oC or 3-(dimethylamino)azetidine dihydrochloride, K_2CO_3, MeCN, rt (c) i. n-BuLi, THF, -78 ^oC, ii. 4-(R^2)-ArCN, THF, -78 ^oC or i. n-BuLi, THF, -78 ^oC, ii. 4-(R^2)-ArCN, THF, -78 ^oC, iii. TFA/DCM (1:2), rt.

TABLES

Table 1. SAR of 3-aryl-5-substituted isoquinolin-1-ones

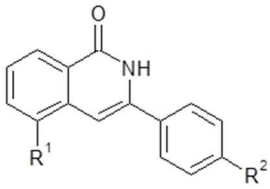

Compound	R^1	R^2	TNKS IC_{50} (nM)	TNKS 95% CI (nM)	WNT-Luc IC_{50} (nM)	WNT-Luc 95% CI (nM)
10	Methoxy	Fluoro	104	92 - 117	120	77 - 186
11	Methoxy	Methyl	34	23 - 50	59	50 - 70
12	Methoxy	CH_2NMe_2	19	17 - 23	136	108 - 170
13	Chloro	Trifluoromethyl	128	101 - 162	483	313 - 744
14	Chloro	CH_2NMe_2	151	136 - 167	364	235 - 566
15	Fluoro	CH_2NMe_2	16	13 - 19	1730	621 - 4790
16	H	CH_2NMe_2	18	16 - 21	>10000	Not applicable

Table 2. SAR of 3-aryl-5-methyl isoquinolin-1-ones

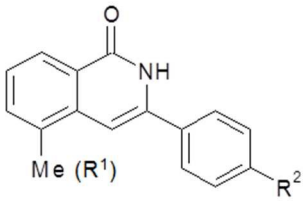

Compound	R^2	TNKS IC_{50} (nM)	TNKS 95% CI (nM)	PARP1 IC_{50} (nM)	PARP1 95% CI (nM)	WNT-Luc IC_{50} (nM)	WNT-Luc 95% CI (nM)	*APC*^{mut} SF_{50} DLD1 (nM)*	DLD1 95% CI (nM)
17	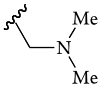	12	9-16	267	224-318	72	37-140	1000	554-2040
18	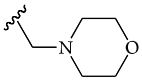	12	10-15	ND	ND	25	23-28	ND	ND
20	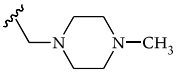	17	15-18	652	470-905	43	27-68	886	645-1220
21	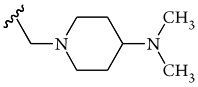	13	9-20	465	376-576	61	51-75	80	59 - 108
22	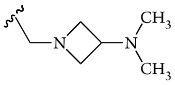	21	14-30	ND	ND	35	27-46	ND	ND
23	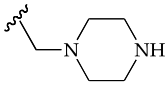	17	12-24	ND	ND	117	73-170	2521	1150- 5526

* ND = Not determined